Canadian Journal of Civil Engineering

Research Article

Mitigating scour in aging run-of-river hydropower infrastructure: an analysis of pressure fluctuations in the physical model of Chancy-Pougny (Switzerland)

Tobias Kurth[a,b,c], **Davide Wüthrich**[b], **Rafael Duarte**[d], **and Giovanni De Cesare**[a]

[a]Hydraulic Constructions Platform, Ecole Polytechnique Fédérale de Lausanne, Switzerland; [b]Department of Hydraulic Engineering, Delft University of Technology, the Netherlands; [c]Aegerter & Bosshardt AG, Basel, Switzerland; [d]Direction Générale de l'Environnement, Canton Vaud, Switzerland

Corresponding author: **Davide Wüthrich** (email: d.wuthrich@tudelft.nl)

Abstract

Many run-of-river hydropower plants built without stilling basins now experience progressive scour due to prolonged operation and increasingly frequent floods. The Chancy-Pougny dam on the Rhône River, constructed in the 1920s at the Swiss–French border, exemplifies this issue. Severe flow recirculation was identified as the main cause of erosion, with pressure fluctuations increasing between the original and current stilling basin. While earlier work developed scour protection measures through physical modelling and numerical predictions, the present study focuses on analyzing pressure measurements within the stilling basin to assess how fluctuations can be reduced to limit future scour. Effective mitigation strategies include: (1) raising the basin water level, (2) introducing a guidance wall to restore symmetrical flow, and (3) adding various configurations of half-cube concrete prisms to increase roughness and energy dissipation. A life cycle assessment of prism materials and construction methods further supports a sustainable approach to rehabilitating ageing hydraulic infrastructure.

Key words: pressure fluctuations, stilling basin, concrete prisms, scour, hydraulic structures

1. Introduction

Many hydropower plants have been in operation for decades. Due to climate change, (severe) floods are expected to become more frequent in the future, implying that spillover events will occur more often (Ruiz-Villanueva and Molnar 2020; Mott et al. 2023). In such situations, the energy associated with these additional discharges is dissipated in spillways and stilling basins. Historically, it was accepted that many of these basins developed naturally into the riverbed, often resulting in scour holes with uncontrolled geometries (Mason and Arumugam 1985). However, progressive scour may require spillway refurbishment, particularly in older schemes (Le Franc 1992; Hernandez et al. 2023) and in downstream areas with unlined riverbeds (Hoffmans and Pilarczyk 1995). Burdekin Falls, Boondooma, Borumba, and Julius dams are some Australian structures prone to scour, which show the globality of the issue (Bollaert and Lesleighter 2014). To ensure long-term safety and reliable operation of these hydraulic structures, scour must be monitored and limited to prevent potential foundation failures. Efficient approaches include adjusting gate operation and enhancing the stilling basin's bottom roughness (Fauconnier 1958), as well as increasing the symmetry by guiding the flow with lateral walls, which can also reduce scour in stilling basins (Kumala et al. 2018; Wüthrich et al. 2021).

Designing or adapting stilling basins is challenging due to the complexity of the phenomena involved. The highly turbulent flows and the resulting pressure fluctuations at the water–rock interface and inside rock fissures depend on Froude, Reynolds, and Weber numbers, making empirical formulations difficult to apply (Duarte et al. 2016). Thus, investing in physical modelling typically becomes necessary. These reduced-size experiments have often led to the implementation of scour-impeding riprap layers, e.g., on Beaumont-Monteux (Derrien et al. 2019), Poses-Amfreville (Sixdenier et al. 2017), and Cusset dams (Barcouda and Guene 2004). For the latter, rock blocks and concrete prisms together formed a riprap layer that proved its stability during laboratory tests. Combined with numerical models, physical experiments can become even more performant, providing a comprehensive assessment of the long-term behavior of the hydraulic structure (Wüthrich et al. 2018).

This manuscript focuses on rock scour induced by dynamic pressures, which in stilling basins originate from jets plunging down from the gates (Bollaert and Schleiss 2005). These pressures can fracture and displace the rock/stone revetments protecting the basin. Therefore, effective scour mitiga-

Fig. 1. The Chancy-Pougny dam and powerplant. From foreground to background: (intended) ship-lock, four-gate-spillway (N°1 in rehabilitation), wall separating stilling basin and powerhouse with restitution channel (photo: T. Kurth).

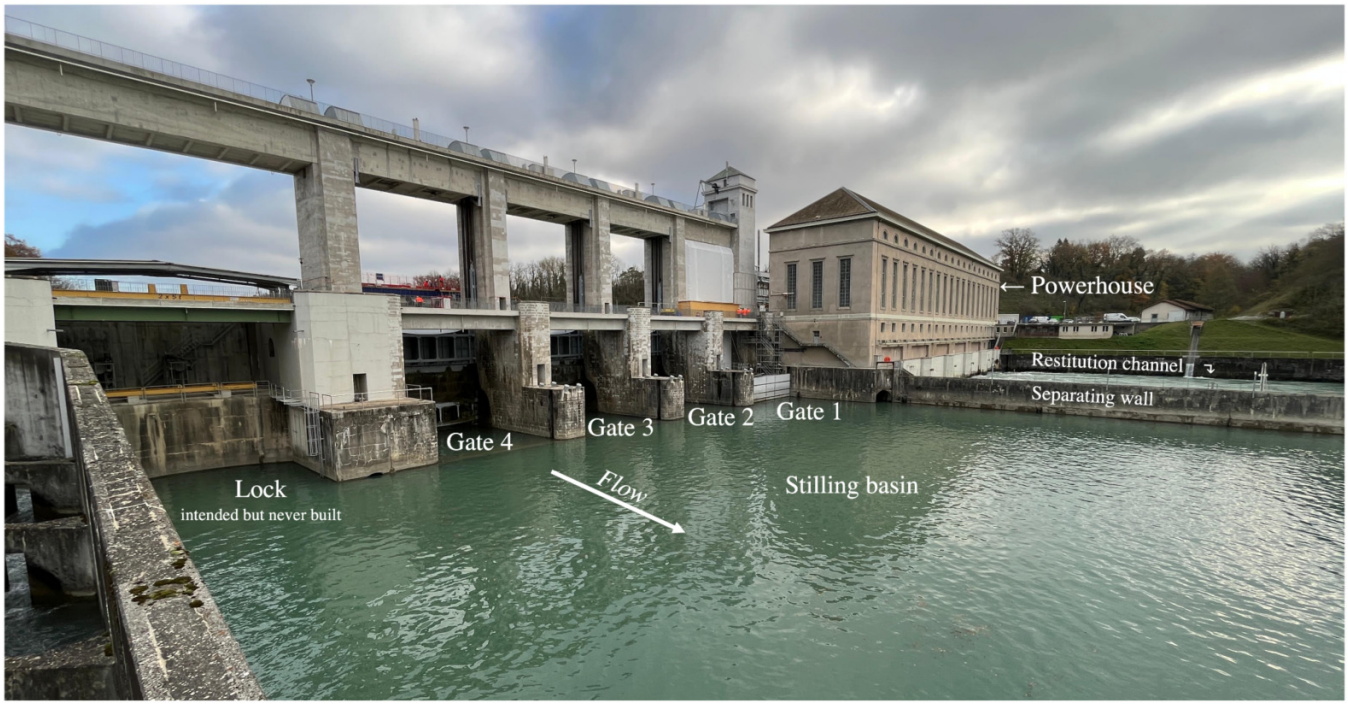

tion strategies should prioritize reducing these fluctuations. Non-dimensional parameters such as hydrodynamic pressure coefficients C_P (mean pressure) and C_P' (standard deviation) have been established based on dynamic similarity (Ervine et al. 1997), permitting the development of simplified models. While these demonstrate high accuracy for C_P, "*available empirical models are not as effective in predicting the C_P' coefficient*" (Fatahi-Alkouhi et al. 2023). Although artificial intelligence finds its application in the numerical prediction of pressure fluctuations (Güven et al. 2006) and scour (Rathod and Manekar 2023), significant gaps in understanding the hydrodynamic behavior of stilling basins persist and predicting pressure fluctuations as a function of anti-scour measures remains challenging. For that, experimental data are highly valuable, as it was the case for Chancy-Pougny (Switzerland).

1.1. The case-study of Chancy-Pougny

Chancy-Pougny is a run-of-river dam situated on the Rhône River, 20 km downstream of Geneva. Built in the 1920's on the Swiss–French border, the hydropower plant has a 10 m head and an installed capacity of 49 MW, resulting in 240 GWh of yearly production. The spillway was conceived without a specifically designed stilling basin (Fig. 1), implying that scour erosion occurred during past spillover events on the downstream riverbed, which consists of weak marls and sandstones. This continuous erosion might endanger the dam's stability in the future (Fig. 2*d*) and the authorities identified scour protection as a critical aspect, commissioning a physical model study to EPF Lausanne (Wüthrich et al. 2021). For that, a 250 m river section containing the facility (Fig. 2*e*) was reproduced in a 1:55 reduced-scale physical model. The initial (1926) as well as an additional bathymetry based on the ensemble of deepest scour depths obtained between 1924 and 2014 (herein referred to as "*minimum elevation bathymetry*") were tested by Wüthrich et al. (2021). This study uses the same dataset.

A strong recirculation current (Fig. 4*a*) was observed during spilling events, both in the physical model and in the prototype. This current was due to a dead-zone caused by an intended (but never built) ship lock. The severity of this re-circulation possibly caused a deep scour hole, which is found in the prolongation of the pillar separating gate 3 and 4 (Fig. 1). Wüthrich et al. (2021) tested various scour protection measures, including (1) a raised basin water level, (2) an anti-recirculation wall, with the goal of "*breaking*" the return flow (Fig. 5), and (3) installation of enhanced bottom roughness in form of rip-rap prisms casted in concrete (Fig. 4). Flow and block movements were visually interpreted while bottom pressure and water level were recorded throughout the stilling basin. These data served as calibration input for a numerical model (Wüthrich et al. 2018), estimating the future scour potential of the different measures.

1.2. Objectives

While Wüthrich et al. (2021) only focused on visual observations and global prism stability, the present study analyzes for the first time the pressure data. The aim is to investigate how each measure contributes to reducing the pressure fluctuations in the basin, therefore improving the scour protection strategy for Chancy-Pougny. More specifically, the main objectives are:

Fig. 2. (Top-left) Orthophoto with position of the profiles and transducers. Numbers represent row (profile) and columns of the transducers with 2.0, 3.0, 4.0, and 5.0 being closest to the dam toe; (*d*) longitudinal cross section at profile 4, where max scour was observed between the initial bathymetry and the minimum elevation bathymetry (values at prototype scale). (*e*) Position of the UltraSonic (US) sensors. Borders of the figure indicate the Rhône section reproduced by the physical model (background from: map.geo.admin.ch).

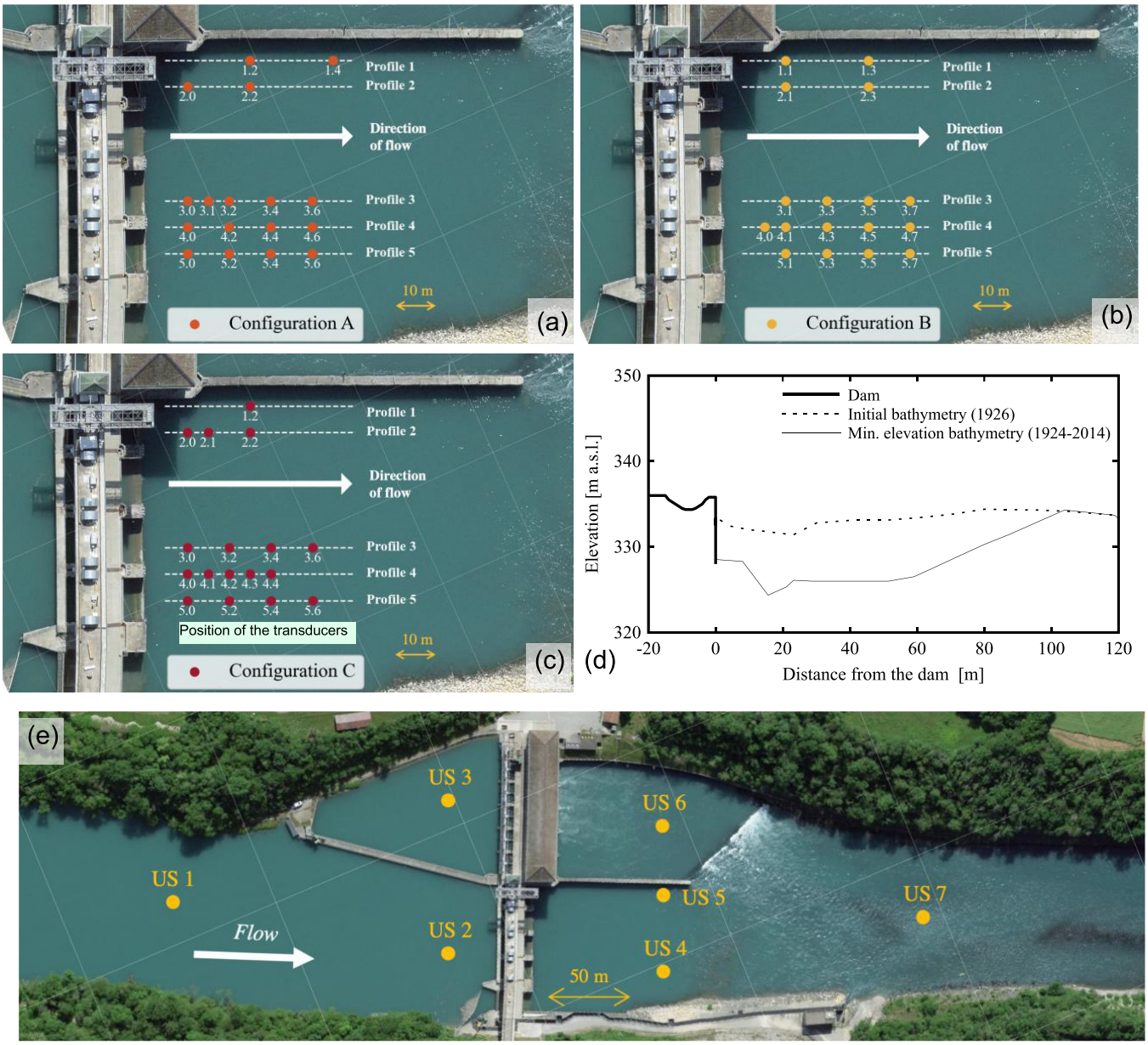

1. Analyze how progressive scour over 100 years of operation affects pressure distributions, including the effect of a higher downstream water level on pressure fluctuations within the stilling basin;
2. Assess the efficiency of various anti-scour measures, including concrete prisms, on reducing pressure fluctuations;
3. Evaluate the environmental impact of these measures through a life cycle analysis.

Additionally, valuable insights and recommendations from this case-study are likely applicable to similar hydraulic schemes, increasing their relevance in the civil engineering community.

2. Methodology

2.1. Physical modelling

In line with Wüthrich et al. (2021), this research used physical modelling to reproduce the processes in the stilling basin. The setup replicated the spillway, powerhouse (inlet and restitution channels), as well as upstream and downstream reaches, ensuring representative inflow and outflow

Table 1. Flow conditions applied on the physical model. Note that values are at prototype scale.

Discharge Q_P (m^3/s)	Return period (years)	Upstream water level (m a.s.l.)	Downstream water level (m a.s.l.)	Elevated DS water level (m a.s.l.)	ΔH (m)	$\Delta H_{elevated}$ (m)
550	<1	347.1	336.4	338.8	10.6	8.3
1080	4	346.1	337.7	340.2	8.2	5.9
1575	100	345.0	338.4	341.4	6.4	3.6
2400	PMF	345.3	341.0	–	4.2	–

Note: Data are at prototype scale. Note that upstream water level refers to US1 and downstream to US7 (Fig. 2).

conditions. The 1:55 physical model integrated two different geometries representing the stilling basin at two points in time:

1. The initial bathymetry, based on surveys established after construction in 1926;
2. A simplified bathymetry, representing the minimum elevations registered over the entire period of operation (i.e., 1926 to 2014), here called "*minimum elevation bathymetry*" and revealing a shape similar to an ellipse (Wüthrich et al. 2021).

Bathymetry data collected by *Société des Forces Motrices de Chancy-Pougny* (SFMCP) with multibeam sonars show that over the years scour eroded over 5 m of the basin bottom (Fig. 2*d*, at prototype scale). To analyze this process, 32 locations were identified within the basin, both along the wall separating the powerhouse (profiles 1 and 2) and in the area downstream of gates 3 and 4 (profiles 3–5), which was the most affected by scour. These locations were investigated using two complementary configurations: A (Fig. 2*a*) and B (Fig. 2*b*), each with 17 piezoresistive pressure transmitters, measuring pressures at the bottom of the stilling basin. Configurations A and B were then combined in configuration C (Fig. 2*c*) to only cover locations of the basin that were identified as most relevant. Membrane-type pressure transducers (Haenni ED701, Baumer PBMN24) were initially employed, later replaced with pinhole-type sensors (Keller PR25) to avoid damage during experiments with moving prisms. Pressures were sampled (at laboratory scale) for 66 s at 1 kHz and repeated six times. Additionally, water levels were recorded using seven ultrasonic (US) sensors (Fig. 2*e*), registering values between 0.1 and 1 m with a response time <80 ms. Water level data were also time-averaged over 66 s (laboratory scale).

2.2. Scaling and similitude

The phenomena under study are difficult to reproduce without substantial scale effects. Jet air entrainment depends on Weber, Reynolds, and Froude numbers. Moreover, the fluid interactions on the rock mass follow Strouhal similitude. Strictly speaking, experimental results of rock scour due to the impact of high-velocity jets obtained on a reduced-scale model cannot be directly extrapolated to prototype conditions. On the other hand, Chancy-Pougny is a low-head facility and given the relevance of gravitational forces in the flow, Froude similitude was applied to guide the experimental design and the scaling of results (Wüthrich et al. 2021). This realistic approach is similar to many other studies in the field of research on rock scour and ensures that the ratio of inertial to gravitational forces remained consistent between model and prototype, allowing accurate reproduction of most relevant physical processes. A geometric scale ratio of 1:55 was used, meaning that prototype values were converted to model values (and vice versa) according to Froude scaling. To facilitate upscaling of the results, pressure data were normalized using the total head difference between upstream (US1) and downstream (US7), defined as $\Delta H = H_{US1} - H_{US7}$, with $H = z + h + V^2/2g$ where z is the bed elevation, h the flow depth, and V the cross-sectional average velocity. $\Delta H_{elevated}$ denotes the configuration with a higher downstream water level (Section 2.3). All values are reported in Table 1.

2.3. Flow conditions

All tests in the physical model were conducted for four discharges, covering a wide range of return periods, from less than 1 year to the probable maximum flood (PMF). These discharges are associated with specific water levels up- and down-stream, detailed in Table 1. Additionally, an elevated downstream water level (DS, measured at US7) was imposed to reproduce an adaptation of the downstream water level that occurred during the operation of the powerplant. Details are provided in Table 1, with values at prototype scale.

For all configurations, the flow within the stilling basin exhibited a strongly turbulent behavior. The jet issued from the gates, characterized by a relatively low head of 10 m, impinged into the stilling basin at a rather flat angle θ, leading to the formation of a (submerged) hydraulic jump (Fig. 3). This hydraulic jump induced significant free-surface fluctuations and intense air entrainment within the stilling basin. Additionally, a secondary recirculation was observed beneath the jet, extending upstream and potentially reaching the dam's vertical wall. When combined with the (horizontal) recirculation caused by the asymmetry of the stilling basin (Fig. 4*a*), these factors created complex three-dimensional dynamics, which strongly affected the pressure distributions within the stilling basin and therefore the effectiveness of scour protection measures, which is the objective of this study.

2.4. Experimental program

Multiple scour protection measures were developed and tested on the physical model by Wüthrich et al. (2021) at a reduced scale 1:55. Besides the anti-recirculation wall (Fig. 5), half-cube prisms of different sizes (Fig. 4*b*) were installed in the stilling basin. Two prism sizes were tested, with edges of

Fig. 3. (*a*) Definition sketch of the jet and (*b*) picture for a prototype discharge $Q_P = 2400$ m^3/s ($Q_M = 107$ l/s), with the initial bathymetry (1926) (photo: D. Wüthrich).

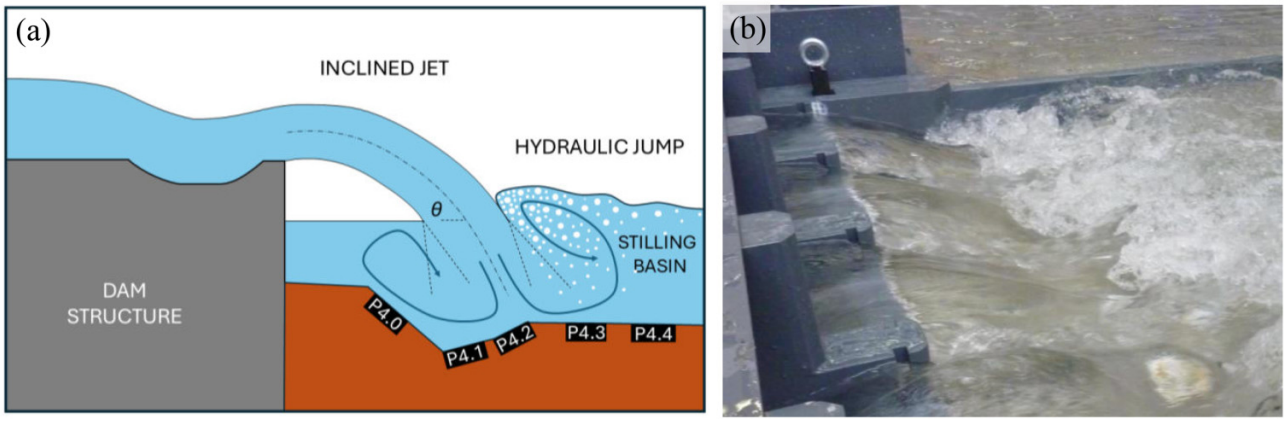

Fig. 4. (*a*) Image of the recirculation on the right bank of the stilling basin; and (*b*) prisms used for the physical modelling. (Bottom) Prism characteristics at prototype scale, assuming 1:55 scaled model (photos: D. Wüthrich).

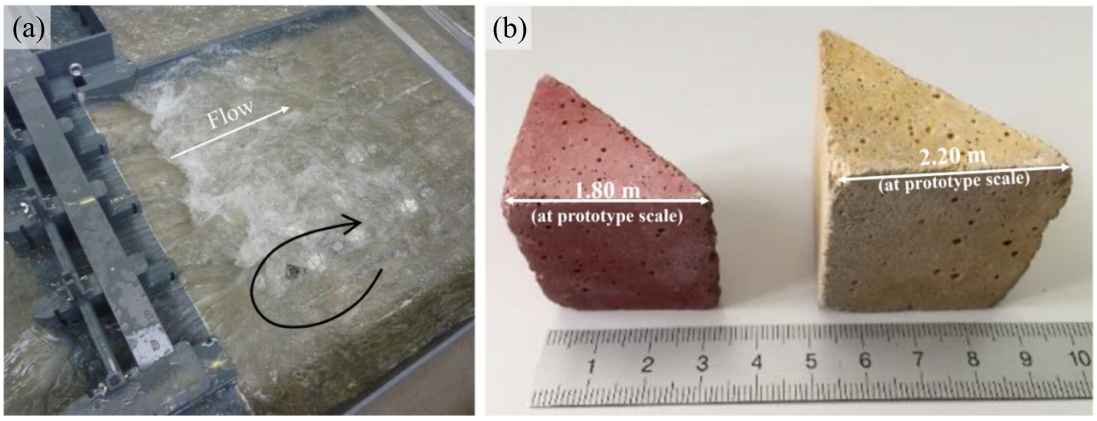

Type	**Size** [m]	**Volume** [m^3]	**Density** ρ [kg/m^3]	**Mass** [kg]
Small (red)	1.8	2.91	2,350	6,853
Large (yellow)	2.2	5.32	2,150	11,447

1.8 and 2.2 m, representing blocks of 6.8 and 11.4 tons (prototype), as detailed in Fig. 4. The prisms had densities slightly lower than commercial concrete (~2450 kg/m^3), without rebars, representing a conservative approach.

The experimental program was divided into four stages:

- **Stage 1**: flow assessment without constructive measures for both the initial bathymetry (Stage 1a) and the minimum elevation bathymetry (Stage 1b). For Stage 1b different downstream water levels were tested.
- **Stage 2**: installation of the anti-recirculation wall to ensure symmetrical flow conditions in the stilling basin (Fig. 5).
- **Stage 3:** various prism layouts were investigated in the physical model (Table 2). Note that Stages 3a to 3e all maintained the anti-recirculation wall.
- **Stage 4**: the optimized prism layout (stage 3e) was tested without the anti-recirculation wall, allowing for an independent analysis of this prism configuration.

2.5. Data analysis

Pressure measurements on the physical model were conducted for 66 s at 1 kHz (laboratory scale) and repeated six times. This led to large datasets that were analyzed using statistical distributions in the form of histograms to visualize mean and fluctuating behaviors (Fig. 6). This approach is visually more impactful than relying on scalar indicators (e.g., pressure coefficients C_P and C_P') and fits better the purpose of this study. However, since the shape of histograms is affected by bin width (e.g., Fig. 6*b*), *violin plots* offer an alternative solution, where the density of data points is indicated in the

Fig. 5. Spillway and stilling basin (minimum elevation bathymetry) of the physical model with the anti-recirculation wall (Wüthrich et al. 2021). Pressure transducers are arranged in Configuration B (photo: D. Wüthrich).

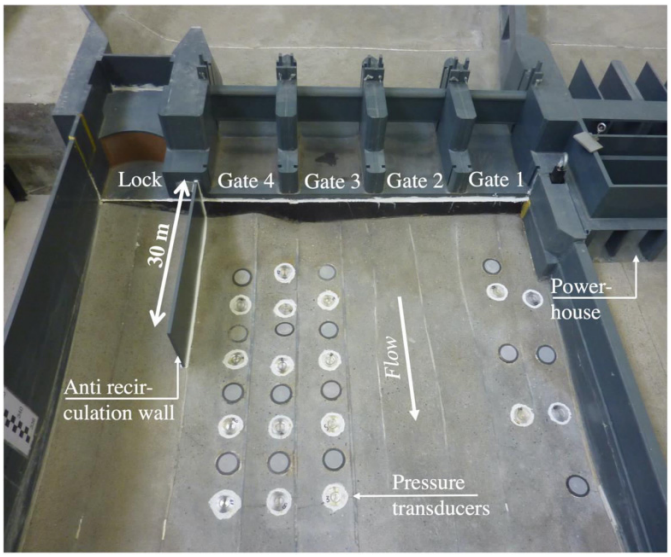

vertical axis, resulting in a shape reminiscent of the musical instrument (Fig. 6*c*). The density is calculated using the Kernel-Density-Estimation (KDE), which is a non-parametric method developed for signal processing (Rosenblatt 1956; Parzen 1962). For violin plots, smoothing is performed algorithmically and it is controlled by the KDE bandwidth, calculated for each dataset according to Silverman (1998). Direct comparison is achieved by plotting two datasets facing each other, sharing the same vertical axis (Fig. 6*c*). A comparison between a histogram and the violin plot using Silverman's approach is shown in Fig. 6*c*, showing the effectiveness of this approach. Adding mean value and quartiles as dashed and dotted lines further improves a violin plot's readability. Spatial interpretation is obtained by locating the violin plots at their specific position along the longitudinal profiles (Fig. 2).

Water levels and pressures were recorded at all locations in Fig. 2. However, flow aeration in the hydraulic jump and strong fluctuations introduced bias in the water depth measurement. To address this, pressure data were shifted relatively to reference locations unaffected by air entrainment, e.g., US5 (in the stilling basin) and US7 (downstream) in Fig. 2. This shift also subtracted the mean (hydrostatic) pressure value at US7 or US5 (in m a.s.l.), isolating the hydrodynamic component of the total pressure (in m w.c.). Consequently, some values appear negative due to the strongly three-dimensional flow conditions within the stilling basin, as detailed in the next sections.

3. Results

3.1. Minimum elevation bathymetry

The first objective was to assess the pressure distributions in the stilling basin with the minimum elevation bathymetry. Data for $Q_P = 2400$ m^3/s (PMF) are shown in Fig. 7, where histograms show higher means between transducer 4.0 and 4.2 (which coincides with the landing point of the jet) and decreasing standard deviation from upstream (transducer 4.0) to downstream (transducer 4.7), indicating greater variability and higher pressure fluctuations in the upstream part of the basin. This observation correlates with the location of deepest scour at transducer 4.1 (Fig. 7), demonstrating that increased scour is associated with higher pressure fluctuations. Data for transducer 4.0 were recorded twice (config. A + B), showing good repeatability.

3.1.1. Effect of stilling basin evolution

Two stilling basin bathymetries were built to calibrate the numerical model (Wüthrich et al. 2018). For this purpose, experiments with an initial (1926) and minimum elevation bathymetries were conducted without any constructive measures (i.e., stages 1a and 1b in Table 2). Data were used to compare pressure fluctuations in the basin at two different points in time. Figure 8 shows that pressure fluctuations increased in the basin's center (i.e., upstream part of profiles 3 and 4), while they reduced near the banks (i.e., profile 1 and profile 5), suggesting a change in dynamics within the stilling basin and the reach of an equilibrium with a higher scour potential in the center. Consequently, this central region is identified as the most critical and profile 4 is considered as the most representative for further examinations, especially for larger discharges. The increase in fluctuations is most likely caused by a modified underwater energy dissipation process, which evolved over the years. Since the spillway jet impinged over a lower bottom (due to the progressive erosion between initial and minimum elevation bathymetry, Fig. 2*d*) the features of the hydraulic jump changed, resulting in water levels ~1 m lower, despite the downstream water level at US5 and US7 being (almost) identical. A lower water level in the basin gave a longer jet, reaching further downstream. Moreover, the jet penetrated in a deeper pool, since the modified hydraulic jump was combined with an important bottom erosion (~5 m, Fig. 2*b*), implying that the jet could better diffuse in the plunge pool (Fig. 3). Altogether, these effects explain why mean pressures and fluctuations increased in the upstream part of the stilling basin during the progression of the scour hole (Fig. 8*a*), which was also observed for other discharges, but not shown herein.

3.1.2. Effect of downstream water level

Different downstream water levels were tested for the same (minimum elevation) bathymetry to analyze the effect of a change in operation on the pressure distribution in the stilling basins. As shown in Table 1 the model's boundary condition was adjusted, raising the water level in the stilling basin by ~3 m. Figure 9*a* presents the results for $Q_P = 1575$ m^3/s, demonstrating that pressure fluctuations were significantly reduced for the high downstream water level, particularly in the upstream part of the stilling basin. Standard deviation at location 4.0 decreased from 0.61 m w.c. to 0.13 m w.c. for

Table 2. Flow conditions tested on the physical model for the minimum elevation bathymetry.

Stage	Initial	After Q_P = 1080 m^3/s [Q_M = 48.1 l/s]	After Q_P = 2400 m^3/s (PMF) [Q_M = 107.0 l/s]
3a Geometric, Small Prisms	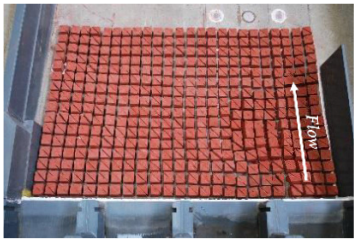		
3b Geometric, Large Prisms			
3c Random, Small Prisms			
3d Random, Large Prisms			
3e Random Half-Half			
4 Random, Final config.			

Note: Results are based on previous findings by Wüthrich et al. (2021). Q_P and Q_M are discharges in the prototype and model, respectively (photos: D. Wüthrich).

Fig. 6. Histograms for: (*a*) 90 bins, (*b*) 30 bins; and (*c*) violin plot comparing different smoothing bandwidths (bw), matching the histogram precision for the same dataset.

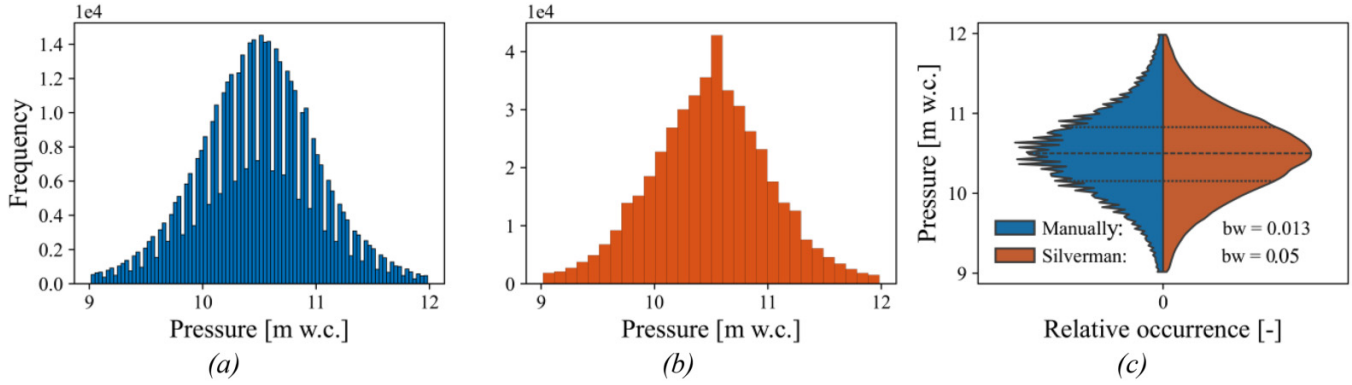

Fig. 7. Pressure distributions at profile 4 for the minimum elevation bathymetry with $Q_P = 2400$ m^3/s. The secondary (inset) axes show total pressures (horizontal) and the number of values per bin (vertical). These are all equally scaled, but labels are displayed only for sensor 4.1.

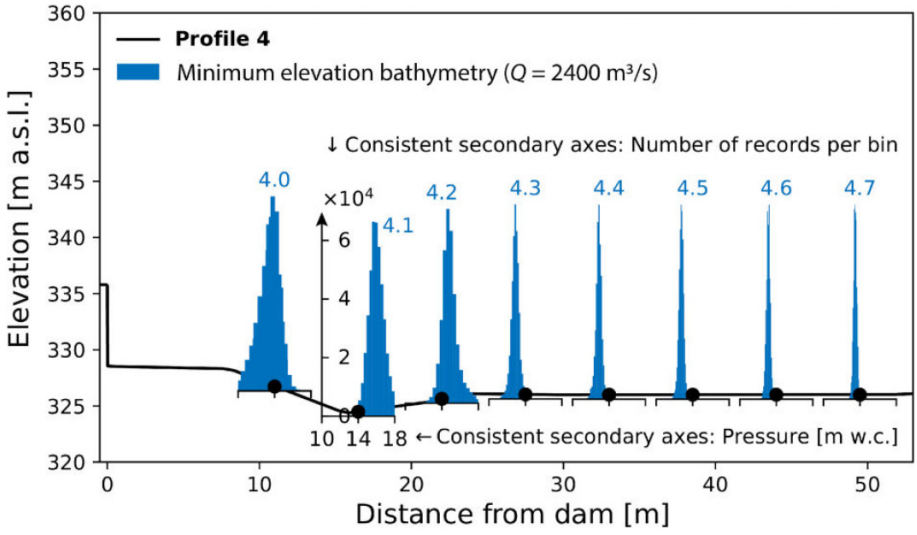

the configuration with higher water level (Fig. 9*a*), confirming that increasing the downstream water level effectively reduces pressure fluctuations. However, it is important to note that changes in downstream water level also affected jet trajectory, altering flow dynamics and mean pressure values in other areas of the basin. This was the case for $Q_P = 1080$ m^3/s (Fig. 9*b*), where slightly higher fluctuations occurred in the downstream section of the basin (transducers 4.4 to 4.6), highlighting the three-dimensionality of scour protection measures and underscoring the need for detailed physical models in such assessments.

3.2. Anti-recirculation wall

The construction of a vertical wall (Fig. 5) was introduced to prevent the formation of the recirculation flow induced by the ship lock's dead-zone (Wüthrich et al. 2021). This approach proved visually effective, resulting in a more straight and uniformly distributed flow (Fig. 10*b*). The addition of the wall altered the dynamics within the stilling basin, including a modified hydraulic jump. While the wall effectively guided the flow, it also reduced the downstream cross-section of the stilling basin, leading to higher water levels. This is supported by a 0.4 m increase in water level recorded at US5, indicating a general rise in water levels which impacted the flow dynamics within the basin. This included the jet, whose trajectory was modified, shifting its impact zone upstream, from transducer 4.1 in the configuration without the wall to transducer 4.0 with the wall, where mean pressures increased. The wall's impact on pressure distributions is analyzed in Fig. 10*c* by comparing data before and after its installation for $Q_P = 2400$ m^3/s. Results show that fluctuations were significantly reduced near the wall (profiles 3, 4, and 5 in Fig. 2*a*), accompanied by increased mean pressures at transducers 4.3 to 4.7. Notably, the standard deviation at 4.0 decreased from 1.16 to 0.15 m w.c., reflecting an ~87% reduction in fluctuations. This indicates generally calmer flow conditions at the bottom, which would help mitigate scour on the right-hand side of the stilling basin.

Fig. 8. Comparison of pressure measurements for the initial (1926) and minimum elevation bathymetries for $Q_P = 2400$ m^3/s (PMF). Data show the hydrodynamic pressure component, with respect to the reference water level at US5 (Fig 3), and normalized using the total head difference ΔH, as indicated on the inset (right) axis. Violins are displayed at the location on the longitudinal profile where they were recorded (Fig. 2*a*). Note that the extent of vertical lines represents the total range of the pressure data, including potential outliers.

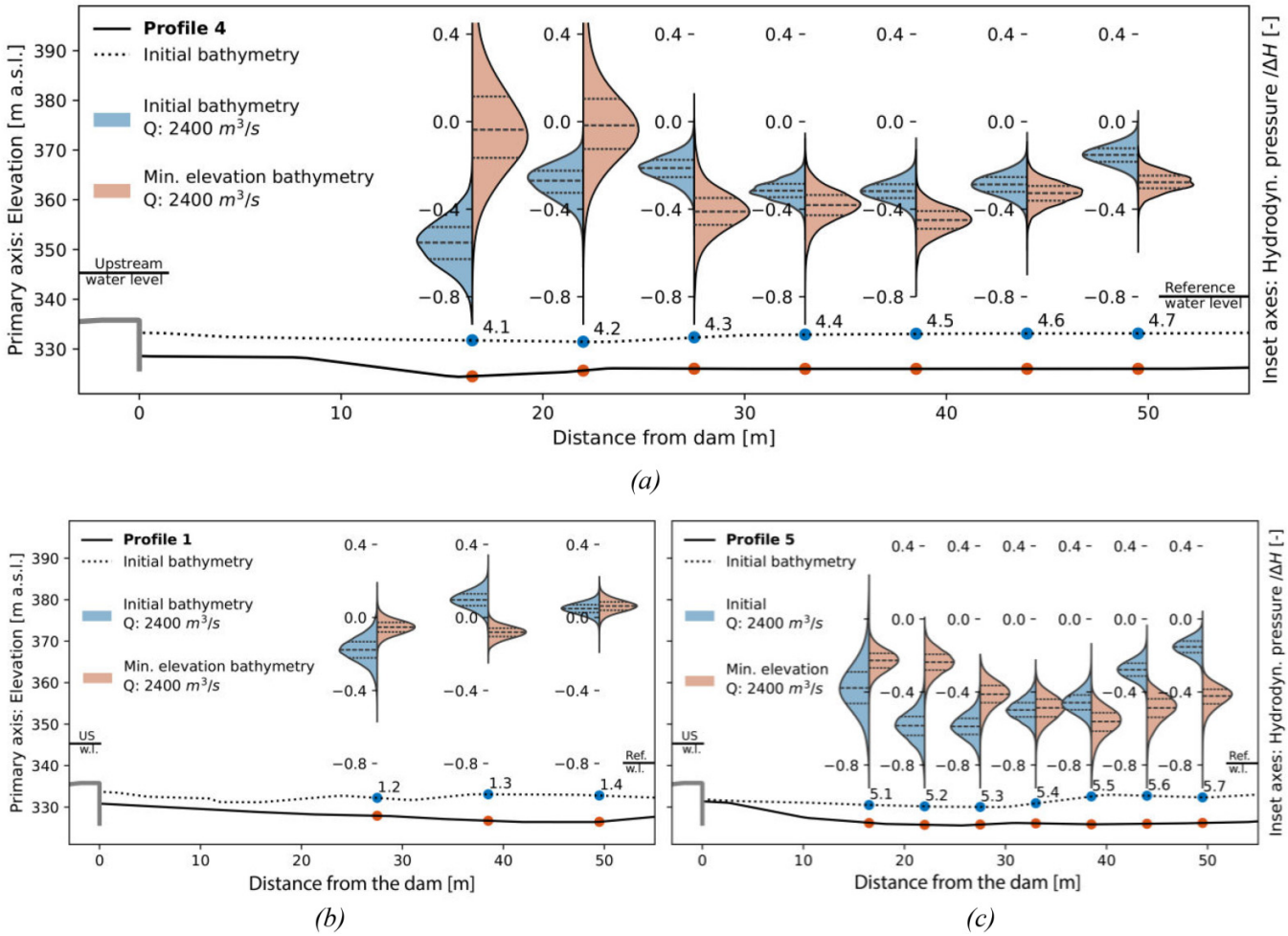

Interestingly, while the reduction in pressure fluctuations near the dam at profile 4 is significant, this change increased the fluctuations on the opposite bank (profile 1, Fig. 10*d*), likely due to the upstream shift of the hydraulic jump. Without the wall, the shape of the hydraulic jump is diagonal (Fig. 10*a*), but with the wall the flow became straight, and the jump moved upstream on the left bank, leading to increased fluctuations (Fig. 10*d*). This confirms the cascading effects that construction measures can have on flow dynamics, underscoring the need for a comprehensive three-dimensional assessment.

3.3. Prism layout combined with wall

To enhance the protection of the stilling basin's bottom, the vertical wall (constructive measure) was combined with the addition of concrete prisms (Wüthrich et al. 2021). These not only increased bed roughness, offering additional protection against abrasion, but also deflected and weakened the jet, enhancing energy dissipation and reducing pressure fluctuations. This makes it particularly valuable to compare the pressure distributions recorded beneath the prism layouts to those of the "*wall only*" configuration (Stage 2).

3.3.1. Geometric prisms layout

Initially, small sized blocks were arranged in the stilling basin with a regular (geometric) pattern tested under a minor discharge ($Q_P = 550$ m^3/s). Wüthrich et al. (2021) showed that this configuration was unstable, with major block movement observed on the left bank (Fig. 11*a*), where pressures recorded by transducer 1.2 exhibited a non-Gaussian bi-modal distribution (Fig. 11*b*). Data were divided into nine subintervals, revealing initially low pressures (Δt_1 to Δt_4). However, during the fifth subinterval Δt_5, block movement occurred, leading to an increase in local pressures (Fig. 11*b*). This resulted in two overlapping distributions, representing pressures before and after the block movement, explaining the unusual shape. Figure 11*a* also shows that some prisms accumulated above transducer 1.2, causing a local increase in water level and explaining the corresponding pressure increase.

Fig. 9. Effect of downstream (DS) water levels on pressure distributions in the minimum elevation bathymetry for: (*a*) $Q_P = 1575$ m^3/s and (*b*) $Q_P = 1080$ m^3/s; blue data represents lower water level, while red data shows an elevated DS water level of ~3 m. Pressure data are normalized using the total head difference ΔH (Table 1).

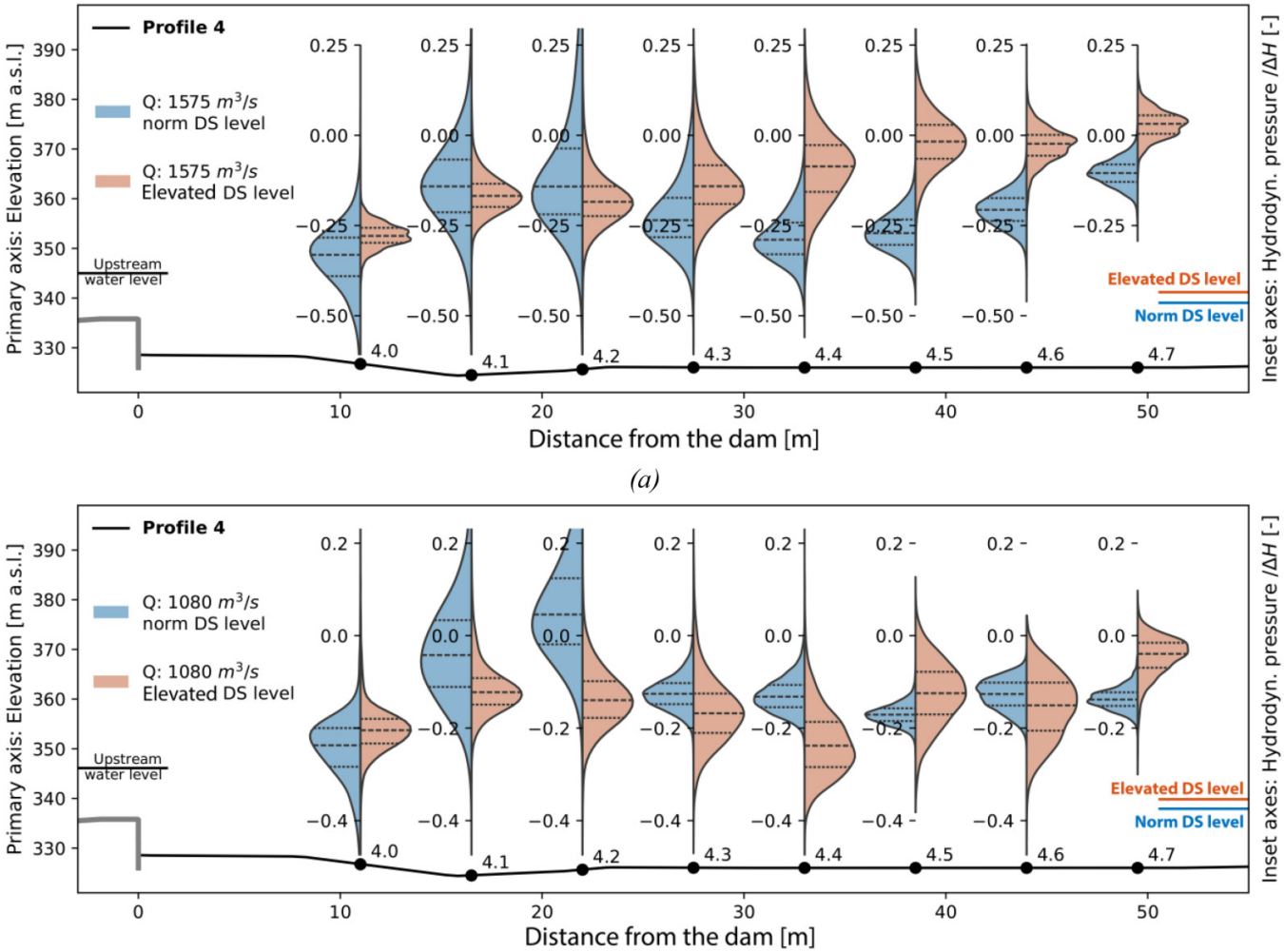

Overall, this geometric layout resulted in minor reduction of pressure fluctuations. Any observed reduction occurred primarily at the beginning of the tests, before any block movement. For larger discharges, a significant number of prisms were displaced (Fig. 11*c*) causing pressure distributions similar to those of the "*wall only*" configuration (Fig. 11*d*). Most notable reduction in fluctuations was found at upstream locations 4.0 and 4.1 (Fig. 11*d*) where the prisms remained stable due to the jet passing above them. Additionally, the prism layer elevated the basin bottom, raising the water level by ~0.5 m and resulting in an increase in mean pressure at transducer 4.0.

Greater stability was achieved by increasing prism size. The layout was redesigned with larger prisms (11.4 tons, Fig. 4), reducing the spatial density from 0.32 to 0.25 prisms/m^2. This new configuration (Stage 3b, Table 2) demonstrated improved stability. During the PMF, the right side of the basin (profiles 3, 4, and 5) showed high stability (Fig. 12*a*), although significant prism displacement occurred on the left side, similar to the smaller prism behavior. However, unlike the smaller prisms, most larger prisms remained within the stilling basin, with only minor displacements. This retention represented an advantage, as the remaining prisms effectively reduced pressure fluctuations (Fig. 12*b*).

In both geometric layouts, underwater videos by Wüthrich et al. (2021) revealed that prism movement did not occur at the start of the experiments, but only after the prisms exhibited a vibrating behavior. Prisms tended to move when adjacent ones were displaced, leaving neighboring blocks directly exposed to the flow. This "domino effect" illustrates that the interlocking arrangement of individual prisms is crucial for stability. For example, a localized increase in pressure fluctuations was observed at transducer 3.2 for $Q_P = 1080$ m^3/s. As the prisms were displaced, this area was no longer shielded (Fig. 11*e*) resulting in increased pressure fluctuations (Fig. 11*f*). Similar amplifications, likely caused by prism rearrangement, were observed in other layouts and locations, but not shown here. To prevent these local increases (which

Fig. 10. Effect of the anti-recirculation wall on the stilling basin with minimum elevation bathymetry: (top) visual observations of the hydraulic jump (*a*) without and (*b*) with the wall. (Bottom) Pressure distributions without (blue) and with (red) the wall: (*c*) profile 4 in the center; and (*d*) profile 1 near the powerhouse (photos: D. Wüthrich).

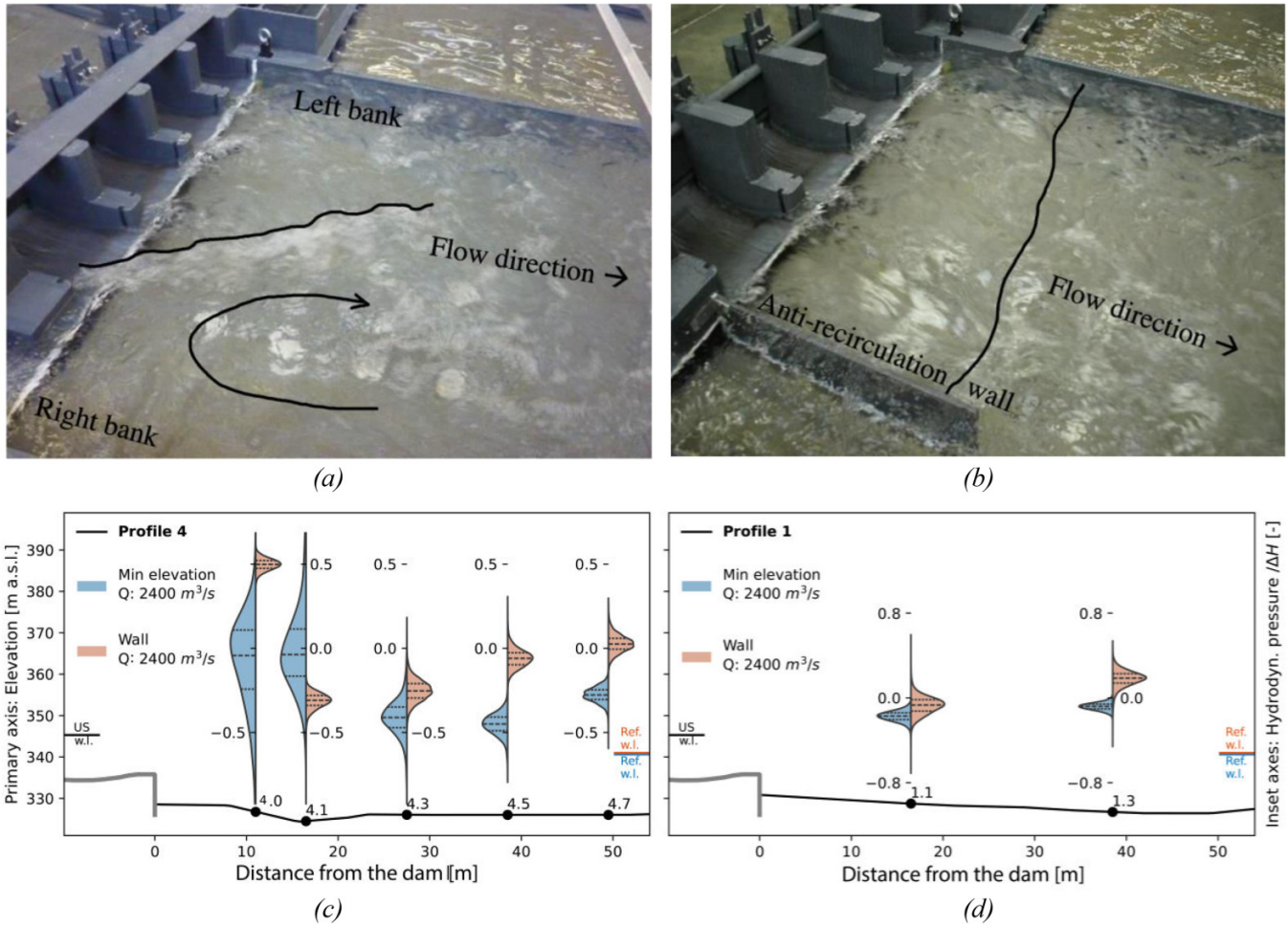

can lead to scour) it is important that prisms remain stable in their positions for design flow conditions, as discussed by Wüthrich et al. (2021)

3.3.2. Randomly arranged prisms

Due to the instability of the geometrical distribution, a random arrangement of the prisms was tested, in addition to the anti-recirculation wall. This approach increased the spatial density to 0.30 prisms/m^2 for larger prisms and 0.43 prisms/m^2 for smaller ones, enhancing their interlocking and entanglement, since many prisms overlapped. Visual observations for the large (random) prisms indicated a more stable carpet (stage 3c, Table 2) with only a few individual prisms washed away on the right side for large discharges. The left side of the carpet remained stable up to the PMF discharge. The presence of prisms also influenced the water levels within the stilling basin, including at US5, thereby affecting the (reference) mean pressure values. With prisms in place, pressure fluctuations were reduced by over 55%, as shown in profile 4 (Fig. 13*a*), where the standard deviation decreased from 0.38 to 0.17 m w.c. at transducer 4.1 and from 0.65 to 0.28 m w.c. at transducer 4.2. The most significant reduction was observed at transducer 4.1, located in the deepest scour hole, highlighting the prisms' effectiveness in mitigating long-term scour.

Similarly, also the small prisms were arranged randomly (stage 3d, Table 2). Observations showed that small red prisms were more stable on the right-hand side of the stilling basin. Since smaller prisms further increased the spatial density, the associated global porosity of the prism layer was lowered, which led to a more effective reduction of pressure fluctuations (Fig. 13*b*). This was particularly evident at transducers 4.1 and 4.2 in Fig. 13*b*, with the most substantial effect observed at transducer 4.2 (77% reduction, with the standard deviation dropping from 0.65 to 0.15 m w.c.), and a significant impact also seen at transducer 4.1 (66% reduction, from 0.38 to 0.13 m w.c.). In comparison, large prisms "only" reduced pressure by 55%.

Wüthrich et al. (2021) showed that large prisms were more stable on the left side of the basin, while smaller prisms had greater stability on the right side. Based on these findings, a "*half–half*" random configuration was developed, combining both setups (stage 3e, Table 2) and increasing the spatial den-

Fig. 11. Pressure distribution for the configuration with small prisms arranged with a geometrical layout (P&W, Geom-S): (*a* and *b*) $Q_P = 550$ m^3/s; (*c* and *d*) $Q_P = 2400$ m^3/s. Subfigures (*e* and *f*) show additional analysis of local increase in fluctuations after block movement ($Q_P = 1080$ m^3/s). Data are compared with the pressure distributions with wall-only. Pressure data are normalized using the total head difference ΔH (Table 1) (photos: D. Wüthrich).

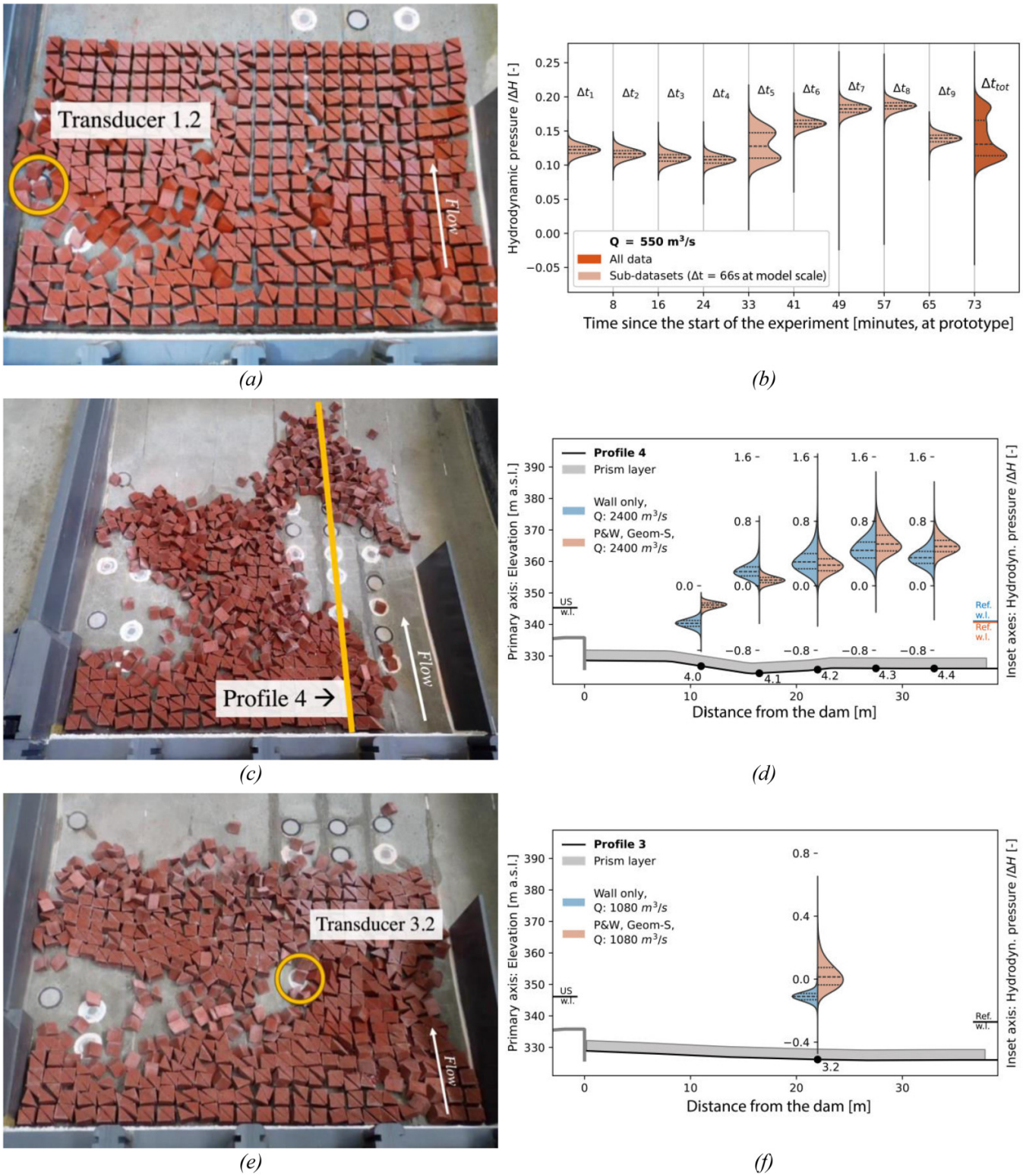

sity to 0.40 prisms/m^2 for large prisms and 0.53 prisms/m^2 for small prisms. This configuration remained stable across all discharges, with only minor movements observed during the PMF ($Q_P = 2400$ m^3/s), mainly on the right side (small red prisms), which was judged acceptable (Table 2). For this new arrangement Fig. 13*c* shows a reduction in pressure fluc-

Fig. 12. Comparison of pressure distributions for the geometrically arranged larger prisms (P&W, Geom-L) and the configuration Wall only during a PMF discharge (Q_P = 2400 m^3/s). Pressure data are normalized using the total head difference ΔH (Table 1) (photo: D. Wüthrich).

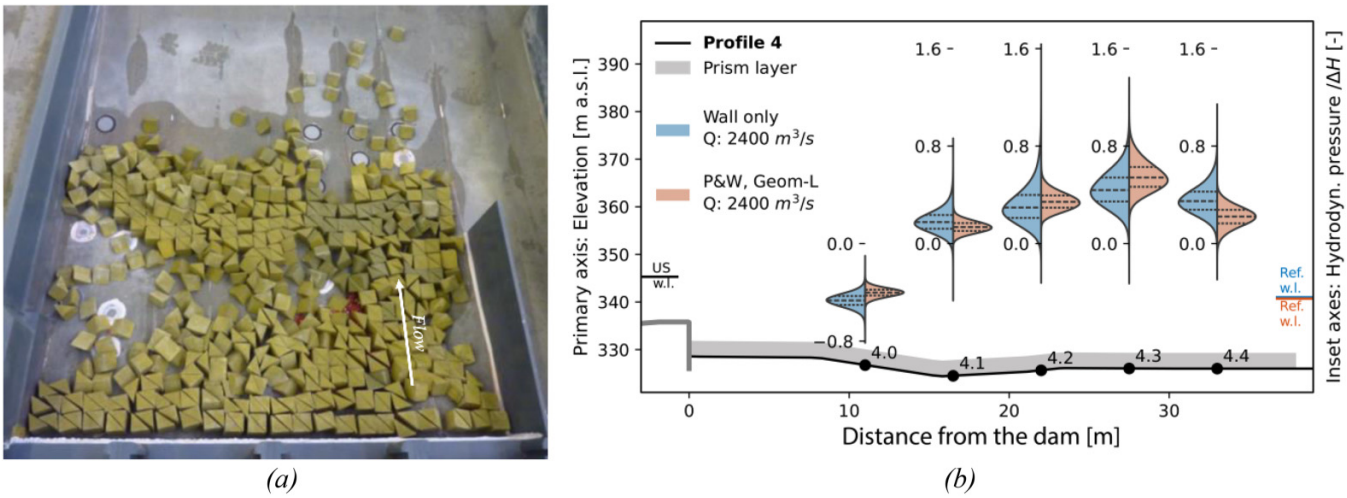

(a) (b)

Fig. 13. Effects of randomly arranged prisms on pressure distributions for various configurations: (*a*) large (random) prisms; (*b*) small (random) prisms; (*c*) half–half (random) configuration (Q_P = 2400 m^3/s); and in subfigures (*a*–*c*) data with prisms (red) are compared to the wall only scenario (blue) along profile 4. Subfigure (*d*) compares pressure distributions at profile 2 for the configuration half–half (stable) and the configuration with random small prisms (unstable) for Q_P = 1575 m^3/s. Pressure data are normalized using the total head difference ΔH (Table 1).

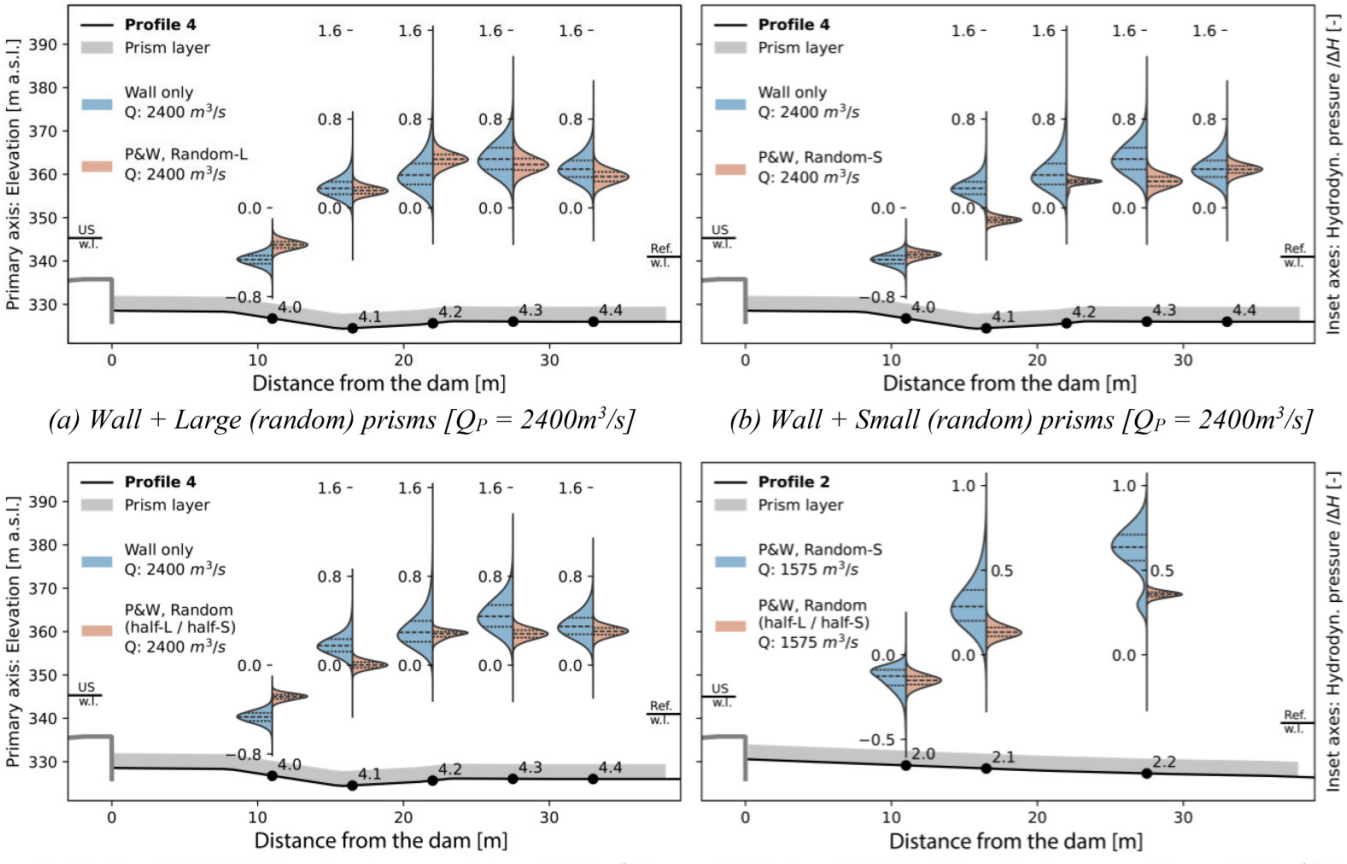

(a) Wall + Large (random) prisms [Q_P = 2400m^3/s] (b) Wall + Small (random) prisms [Q_P = 2400m^3/s]

(c) Wall + Half-Half (random) prisms [Q_P = 2400m^3/s] (d) Wall + Half-Half (random) prisms [Q_P = 1575m^3/s]

Fig. 14. Picture of the configuration and pressure distribution of the optimized prism layout (red) and comparison with the wall only setup (blue). Pressure data are normalized using the total head difference ΔH (Table 1) (photo: D. Wüthrich).

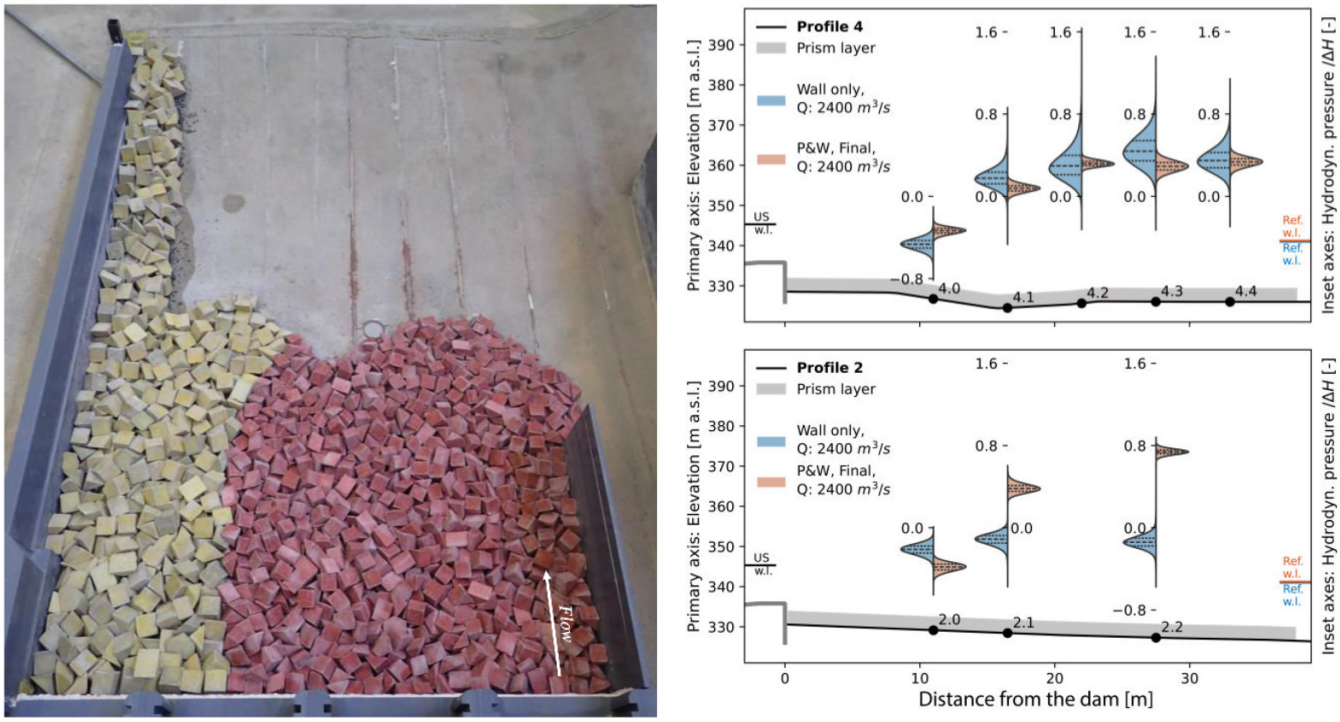

tuations along profile 4 compared to the "wall-only" configuration, as expected. Despite the higher prism density, the extent of fluctuation reduction remained comparable to the earlier configuration with a lower density of small red prisms (Fig. 13*b*). Yellow (large) prisms were installed with a higher density on the left side of the basin (profiles 1 and 2). These large (yellow) prisms remained stable for all discharges (Stage 3e), and their pressure distributions recorded along profile 2 (red data in Fig. 13*d*) showed lower fluctuations compared to the configuration with small randomly arranged prisms (Stage 3d, Table 2), which was unstable for $Q_P = 1575$ m^3/s, specifically at profiles 1 and 2. This is particularly interesting, because it shows the close relationship between stability (addressed by Wüthrich et al. 2021) and pressure reduction, emphasized in this study. Overall, this mixed configuration achieved an efficient reduction of the pressure fluctuations on both sides of the stilling basin. However, while qualitative, these data show promising results, pointing out the need for further studies to better quantify the effects of carpet properties on pressure reduction.

3.3.3. Optimized prism layout

Although the half-half configuration was generally stable, some small (red) prisms were displaced under PMF conditions (stage 3e, Table 2). To address this, the combination containing both prisms was further optimized and a more precise layout was developed based on the actual topography of the stilling basin. While maintaining the anti-recirculation wall, this optimized layout utilized a total of 960 small and 540 large prisms (Fig. 14*a*) and proved stable for all discharges (stage 3, Table 2). The increased roughness reduced flow velocities, causing a rise in water level of ~0.2 m within the basin, as recorded by US5. This rise in water level altered the hydraulic jump, shifting the jet impact zone upstream and affecting mean pressure values, particularly on the left side of the basin. Specifically, this shift resulted in a drop in mean pressure at transducer 4.1 (former impact zone) and a rise at transducer 4.0 (new impact zone). Overall, data showed that pressure fluctuations were effectively reduced (Fig. 14). Unlike the wall-only configuration, which primarily affected the most upstream transducers 4.0 and 4.1 (Fig. 10*c*), this optimized prism layout produced a more widespread effect, reducing fluctuations across all transducers along profile 4 (Fig. 14*b*). Although less pronounced, transducers along other profiles confirmed this trend (e.g., profile 2 in Fig. 14*c*).

3.4. Prism carpet without wall

Demonstrating high stability and effectiveness in reducing fluctuations, the optimized prism layout was also tested without the wall, with the carpet extended with the same density along the natural topography toward the right bank. As a result, no blocks were placed in the area downstream of the ship lock (stage 4, Fig. 15). Visual observations confirmed that recirculation did not occur in the downstream stilling basin, even without the wall. The increased roughness created by the prisms on the plunge pool bottom, was sufficient to mitigate recirculation and restore a more symmetrical flow pattern (Wüthrich et al. 2021). Without the wall, the jet impacted a basin that was no longer laterally confined, causing the water level to drop by ~0.7 m (see US5, Fig. 15). Despite the absence of the wall, data showed that pressure fluctua-

Fig. 15. (Left) picture of the final optimized prisms only configuration (without wall) and (right) pressure distributions under PMF ($Q_P = 2400$ m^3/s) (in red) and comparison with the configuration Prisms and wall (in blue). Pressure data are normalized using the total head difference ΔH (Table 1) (photo: D. Wüthrich).

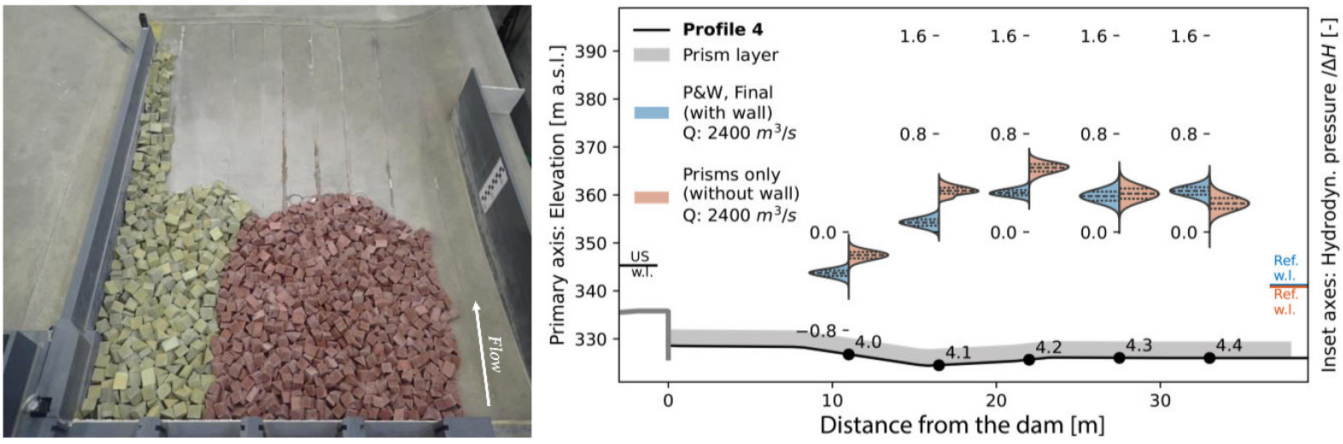

tions remained comparable (Fig. 15), demonstrating the effectiveness of the optimized layout for all flow conditions.

3.5. Summary of prisms behaviour

Many configurations were tested in the laboratory to assess both the stability of the bed protection (Wüthrich et al. 2021) and their influence on pressure distributions (present study), revealing that these two aspects are closely linked. Although this study offers primarily qualitative insights, several key findings can be highlighted. In primis, stilling basins involve highly complex flow conditions, where modifications at one location can produce unexpected consequences elsewhere. If prisms are chosen, then their stability is fundamental, since only when they remain in place can they effectively contribute to reducing pressure fluctuations. In this regard, randomly arranged prisms outperformed geometrically placed ones, providing greater reduction of pressure fluctuations. Introducing prisms also increased flow depths, which modified the jet trajectory and shifted the impact zone. As a result, pressure reductions cannot be evaluated locally, but their behavior within the entire basin must be considered. This highlighted the need for more targeted studies on the role of block arrangement and porosity in pressure attenuation, and underscores the continued importance of physical modeling in advancing hydraulic engineering design.

This also showed that an effective hydraulic solution was found to prevent recirculation and reduce bottom pressure fluctuations, but its feasibility depends on addressing technical, economic, environmental, and social factors. While costs and operations can be refined during project implementation, environmental and social considerations should be integrated at early stages. Therefore, the next section addresses the solution's sustainability.

4. Sustainability

The scour protection measures in Section 3 require many prisms, resulting in substantial concrete usage. This raises concerns about material toxicity, emissions, raw material consumption, and their impact on the global environment of the Rhône ecosystem. To mitigate these effects, alternative materials and construction methods are recommended. Literature and initial calculations indicate that environmental benefits can be maximized by:

1. Minimizing the volume of concrete;
2. Reducing the proportion of cement in the concrete mix;
3. Utilizing eco-friendly cement (eco-cement).

This study highlights that reducing concrete volume lowers environmental impacts and material costs.

4.1. Construction techniques

Concrete volume can be minimized through geometric adjustments of the prisms or by (partially) replacing concrete with alternative materials, as detailed below.

(1) **Infilled prisms**: Hollow concrete prisms, filled with aggregates and sand, can significantly reduce concrete (e.g., Fig. 16), but it introduces greater complexity in formwork and construction. A reduction of the thickness of hollow prisms can be achieved using ultra-high performance fiber reinforced concrete (UHPFRC; see, for example, Habel et al. 2006), which also has high resistance against underwater abrasion (Lochon et al. 2024).

(2) **Natural rocks**: Granite blocks of sufficient size can be sourced from the Swiss or French Alps, presenting an ecological alternative to concrete, not only because it reduces the environmental impact but also provides enhanced stability due to granite's higher density. The proximity of a railway line to Chancy-Pougny facilitates the transport of materials. Additionally, because natural rock blocks are typically irregular in shape, they inherently provide the necessary roughness, avoiding the added costs of casting blocks into specific geometries.

Fig. 16. Reduction of concrete volume as a function of wall thickness. Thirty centimeters for a small prisms is deemed structurally sufficient. Dimensions in cm.

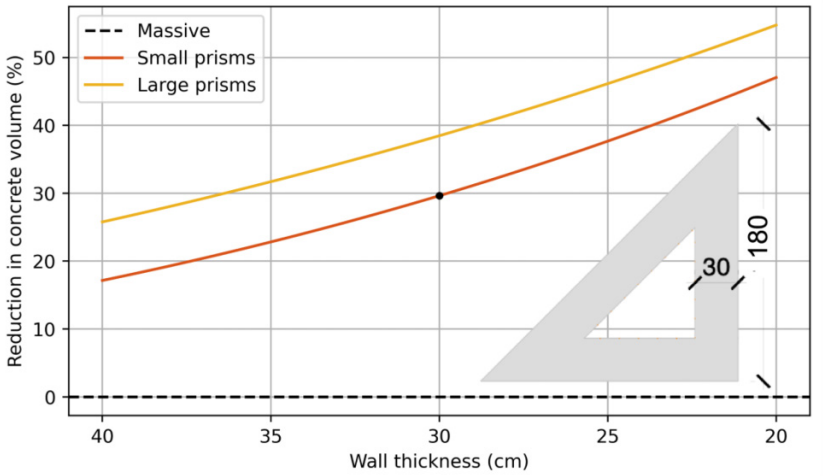

(3) **Gabions**: Steel-wire frames filled with loose rocks can ensure effective hydraulic performance and offer an ecological alternative (Wüthrich and Chanson 2014, 2015). Their environmental footprint largely depends on the amount of steel used. However, ensuring resilience against displacement or impacts from adjacent gabions is critical. This can potentially be addressed by using interconnected units (e.g., welted or binded) or Gabion Mattress, whose technical properties are in continuous evolution. Durability, a primary concern, may be improved using galvanized steel, while the constant submersion of baskets in the basin aids in preserving their integrity. Further enhancements could be achieved by replacing steel wires with composite rebars or glass fiber geogrids, alternatives worth exploring in later stages of the project.

(4) **Armor units**: To enhance interlocking capabilities, coastal protection units have become increasingly refined over the past decades (e.g., Kudale et al. 2021). Recent advancements focused on increasing their slenderness to reduce the required concrete volumes and therefore the associated CO_2 footprint. A similar approach could be applied to Chancy-Pougny, with increased block stability and surface roughness allowing for a reduction in prism size. However, armor units are designed to remain stable on slopes under wave attack, which differs significantly from the conditions of a jet-impacted stilling basin. Therefore, assessing the feasibility of using armor units and determining the minimum size will need specific testing.

4.2. Comparison of alternatives

Life cycle assessment (LCA) is a widely recognized tool to analyze environmental impacts. The global database "*ecoinvent_v.3*" and its implementation for the Swiss construction industry by KBOB (https://www.kbob.admin.ch) provides strong spatial correlation and comparability across various materials and transport modes. The LCA not only quantifies greenhouse gas emissions and energy use of the entire supply chain (i.e., construction, transportation, and installation), but also consolidates a broad range of environmental effects into a single metric called UBP (*Umwelt Belastungs Punkte*, or "environmental impact points"). This metric integrates factors such as energy and material resources, land and freshwater use, emissions to air, water, and soil, waste treatment residues, and traffic noise, weighted according to the Swiss ecological scarcity method and environmental policy (IPB and KBOB 2010). For a meaningful comparison of different alternatives, a functional unit (FU) is defined in each LCA. In this case, the FU is based on the individual block weight[1]. For the other alternatives, LCA results are presented in Fig. 17, with some assumptions. For concrete alternatives (i.e., massive and infilled prisms), emissions related to transportation and types of mixtures are accounted for using KBOB, based on average Swiss usage. Granite blocks are assumed to be sourced from a quarry 350 km away (closest one with sufficient size and volumes), while gabions are conservatively made of a steel wire mesh (e.g., diameter 12 mm and spacing 150 mm). Despite these conservative assumptions, non-concrete solutions clearly show a more favorable ecological profile. LCA results in Fig. 17 are subdivided in multiple categories, including their UBP (environmental impact points), energy use (both renewable and non-renewable) and greenhouse gas emissions. Results indicate that the solution using massive concrete prisms is the least environmentally attractive, due to high UBP scores, CO_2 emissions and energy consumption. These impacts can be reduced by adopting an infilled design, which cuts CO_2 emissions by nearly 500 tons and lower UBP. Replacing concrete with granite blocks improves sustainability, but it highlights the importance of transportation, with road transport having higher non-renewable energy consumption com-

[1] Note that the ecological performance of armor units is directly related to their concrete volume (which requires specific laboratory tests beyond the scope of this study), so armour units are not considered in this LCA analysis.

Fig. 17. Life cycle assessment (LCA) for different construction methods, materials and transport modes, computed using the KBOB methodology for Switzerland (IPB and KBOB 2010).

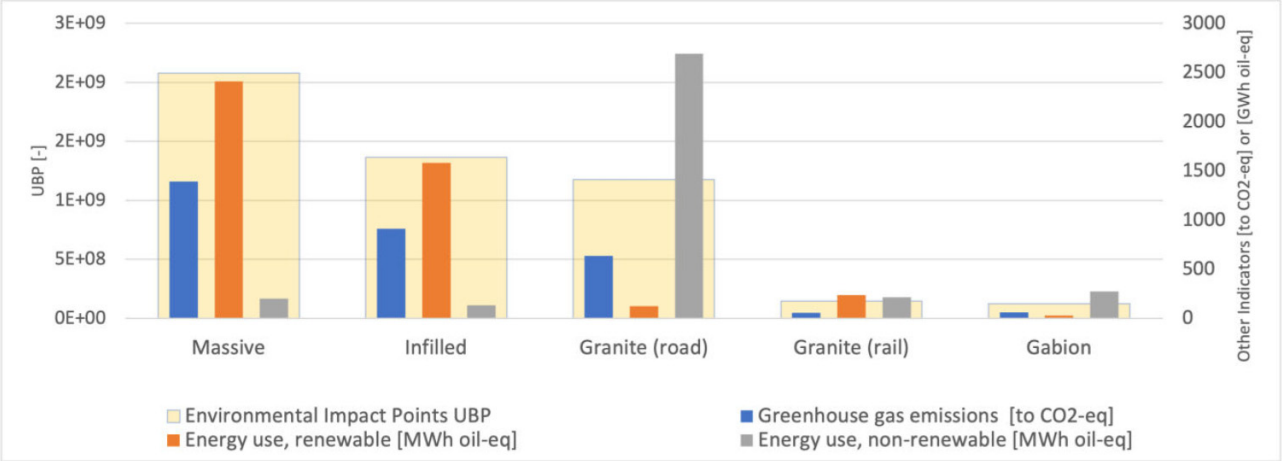

pared to trains. Non-concrete strategies generally demonstrate superior environmental performance and could be further improved by engaging local, experienced contractors. Given the increasing cost of concrete, these alternatives appear to be economically attractive, worth exploring in the future.

4.3. Discussion on sustainability and LCA

Concrete remains a highly effective material frequently used in hydraulic engineering. Therefore, strategies to reduce its ecological impacts are essential to optimize the sustainability of these solutions. Since cement is the primary contributor to the carbon footprint of concrete, its content in the mixture must be minimized while ensuring durability and performance. However, if these reductions result in a shorter prism life, the need for early replacement could negate the initial environmental and cost benefits. In a hydraulic context, abrasion resistance is a critical factor, closely linked to compressive strength, which is directly impacted by a lower cement content. Kryžanowski et al. (2012) established correlations between laboratory tests and observations made on the stilling basin of the Vrhovo hydropower plant on the Sava River in Slovenia. Additionally, a reduced cement content lowers water acidification due to the leaching of calcium hydroxide and other alkali materials, thus further decreasing the environmental impact of concrete. The remaining three-quarters of concrete's volume (the aggregates) also significantly affect its environmental impact. Literature indicates that the efficiency of recycled aggregates, such as crushed end-of-life concrete elements, depends largely on the transport distance and the additional cement required to achieve comparable physical properties (Knoeri et al. 2013). Alternatively, the sediment load carried by the Rhône, along with locally available gravel, could serve as an ecologically viable source of primary aggregate.

Lastly, eco-cements partially replace clinker with limestone (e.g., CEM II/A and CEM II/B), which have lower CO_2 emissions and are comparably priced to conventional Portland CEM I on the Swiss market. Even more environmentally friendly alternatives, like ZN/D or the recently introduced CEM II/C, may not be available at all production sites and typically carry a slight additional cost.

5. Conclusion

Many aging hydropower plants, including Chancy-Pougny, face increasing scour issues due to more frequent and severe floods. Therefore, protective measures have become necessary for safe dam operation. Wüthrich et al. (2021) developed scour protection solutions for the Chancy-Pougny stilling basin by combining numerical estimations with physical modelling. The current study builds upon this work by examining the pressure measurements recorded in the stilling basin of the physical model, focusing on pressure fluctuations. The efficiency of different scour protection measures, involving an anti-recirculation wall and a riprap layer made of artificial concrete prisms was evaluated by distribution-pattern analysis and comparison among different setups. Main findings include:

- Decades of operation led to scour erosion and altered the dynamics of the jets coming out of the gates. The basin's asymmetry, resulting in a return current that interacts with these jets, exacerbates the issue. Comparing pressure data from initial (1926) and a minimum elevation bathymetries reveals increased pressure fluctuations in the central region of the stilling basin, aligning with the deepest scour hole. Conversely, pressure fluctuations near the banks stabilized.
- Data showed that increasing the downstream water level was effective in reducing pressure fluctuations in the stilling basin, particularly in the central areas, more prone to severe scour. However, this adjustment also affected flow dynamics, with increased fluctuations at lower discharges,

highlighting the importance of considering complex flow interactions in scour protection assessments.

- The construction of an anti-recirculation wall successfully straightened the flow, shifting the hydraulic jump upstream and aligning it orthogonally, resulting in a slight increase in water level. This reduced fluctuations at the center of the basin, but they increased along the left bank. These findings suggest that while the wall might effectively mitigate upstream erosion, a more comprehensive consideration of the three-dimensional flow dynamics is necessary to address potential effects at other locations.
- While keeping the anti-recirculation wall in place, two sizes of half-cube-shaped concrete prisms were used to increase bottom roughness and enhance energy dissipation. Geometrically arranged prisms proved unstable, with most blocks displaced by the flow and resulting in little change to pressure distributions. In contrast, randomly arranged prisms demonstrated greater stability, though some displacement still occurred. The most effective approach combined randomly placed smaller prisms in deeper areas with larger blocks in shallower zones, withstanding the PMF. This configuration significantly reduced bottom pressure fluctuations in addition to the improvements already achieved by the wall, proving to be a globally efficient solution for scour mitigation.
- The optimized prism layout was stable and effective even without the anti-recirculation. By preventing the formation of a recirculation current, this solution effectively reduced pressure fluctuations across the entire stilling basin.

These results pointed out the complex nature of flow dynamics in the stilling basin, where solutions implemented in one area can influence flow behavior in other regions. This highlights the importance of accounting for the three-dimensional characteristics of flows when evaluating scour protection measures, emphasizing the critical need for detailed physical models in such assessments.

Lastly, the optimized layout with concrete prisms was evaluated for environmental impact, focusing on reducing concrete volume and cement use. Hollow prisms or armor-unit geometries could reduce concrete use while maintaining stability. Substituting concrete with natural rock blocks would be an effective option, though steel gabions with smaller rocks raised durability concerns. Overall, transport distance and mode significantly influenced environmental effects, with rail transport being the most efficient. This highlights the necessity of integrating hydraulically efficient solutions with environmentally sustainable practices to ensure a sustainable future to hydropower infrastructure.

List of symbols

bw	band width in violin plots [-]
C'_p	dimensionless coefficient to characterize pressures fluctuations [-]
C_p	dimensionless coefficient to characterize mean pressures [-]
g	gravitational constant, here $g = 9.81$ [m/s^2]
h	flow depth [m]
H	total head, computed as $H = z + h + V^2/2g$ [m]. H_{US1} refers to US1, H_{US7} refers to US7 (Fig. 2*e*)
Q	discharge [m^3/s], Q_M refers to the model, while Q_P to the prototype
V	cross-sectional average flow velocity [m/s]
z	elevation [m a.s.l.]
ΔH	total head difference between up- (US1) and downstream (US7), $\Delta H = H_{US1}$ - H_{US7} [m]
$\Delta H_{elevated}$	head difference between up- (US1) and downstream (US7) with elevated water level [m]
Δt	time interval [s]
ρ	density of the prisms [kg/m^3]

Acknowledgements

The authors would like to acknowledge the Société des Forces Motrices de Chancy-Pougny (SFMCP) for commissioning the study, and people involved in the study: Dr. Sabine Chamoun (EPFL, currently at Etat de Genève, Switzerland), Mr. Olivier Vallotton (Stucky SA, Switzerland) and Mr. Etienne Dufey (Stucky SA, Switzerland; currently at Alpiq, Switzerland), Dr. Thierry Bussard (Norbert SA, Switzerland), and Dr. Matthieu Ferrière (CNR, France). The constructive feedback of Dr. Tara Habibi (EPFL, Switzerland) on sustainability aspects is also acknowledged.

Article information

History dates

Received: 16 January 2025
Accepted: 17 September 2025
Accepted manuscript online: 26 September 2025
Version of record online: 17 November 2025
Corrected: 9 March 2026

Notes

The article was originally published with errors that have now been corrected. See Correction: [http://dx.doi.org/10.1139/cjce-2026-0050].

Data availability

Data generated or analyzed during this study are not publicly available due to ownership by the client, but might be available from the corresponding author on reasonable request.

Author information

Author ORCIDs

Davide Wüthrich https://orcid.org/0000-0003-1974-3560
Rafael Duarte https://orcid.org/0000-0001-9657-8429
Giovanni De Cesare https://orcid.org/0000-0002-1117-3180

Author contributions

Conceptualization: TK, DW, GDC
Data curation: TK, DW
Formal analysis: TK, GDC, DW
Methodology: TK, DW, GDC
Supervision: DW, RD, GDC
Validation: RD
Writing – original draft: TK
Writing – review & editing: DW, RD, GDC

Competing interests

The authors declare there are no competing interests.

References

Barcouda, M., and Guene, C. 2004. Déchargeurs du barrage usine de Cusset. La Houille Blanche, **90**(4): 39–45. doi:10.1051/lhb:200404004.

Bollaert, E.F.R., and Lesleighter, E.J. 2014. Spillway rock scour experience and analysis–the Australian scene over the past four decades. *In* 5th international symposium on hydraulic structures. p. 189., Brisbane, Australia.

Bollaert, E.F.R., and Schleiss, A.J. 2005. Physically based model for evaluation of rock scour due to high-velocity jet impact. Journal of Hydraulic Engineering, **131**(3): 153–165. doi:10.1061/(ASCE)0733-9429(2005)131:3(153).

Derrien, S., Clutier, A., Blancher, B., and Carraz, F. 2019. Étude sur modèle réduit des affouillements en aval du barrage de Beaumont-Monteux sur l'Isère. La Houille Blanche, **105**(1): 48–55. doi:10.1051/lhb/2019007.

Duarte, R., Pinheiro, A., and Schleiss, A.J. 2016. An enhanced physically based scour model for considering jet air entrainment. Engineering, **2**: 294–301. doi:10.1016/J.ENG.2016.03.003.

Ervine, D.A., Falvey, H.T., and Withers, W. 1997. Pressure fluctuations on plunge pool floors. Journal of Hydraulic Research, **35**(2): 257–279. doi:10.1080/00221689709498430.

Fatahi-Alkouhi, R., Shanehsazzadeh, A., and Hashemi, M. 2023. Enhanced physically based models for pressure characteristics at plunge pool bottoms. Journal of Hydraulic Engineering, **149**(11): 04023044. doi:10.1061/JHEND8.HYENG-13398.

Fauconnier, B. 1958. Le problème des affouillements à l'aval des barrages. La Houille Blanche, **44**: 123–144. doi:10.1051/lhb/1958026.

Güven, A., Günal, M., and Çevik, A. 2006. Prediction of pressure fluctuations on sloping stilling basins. Canadian Journal of Civil Engineering, **33**(11): 1379–1388.

Habel, K., Viviani, M., Denarié, E., and Brühwiler, E. 2006. Development of the mechanical properties of an ultra-high performance fiber reinforced concrete (UHPFRC). Cement and Concrete Research, **36**(7): 1362–1370. doi:10.1016/j.cemconres.2006.03.009.

Hernandez, H., Azimi, A.H., and Mostaani, A. 2023. Effect of armor layer on the local scour formation induced by a deeply submerged circular wall jet in confined channels. Canadian Journal of Civil Engineering, **50**(6): 510–522. doi:10.1139/cjce-2021-0386.

Hoffmans, G.J.C.M., and Pilarczyk, K.W. 1995. Local scour downstream of hydraulic structures. Journal of Hydraulic Engineering, **121**(4): 326–340. doi:10.1061/(ASCE)0733-9429(1995)121:4(326).

IPB and KBOB. 2010. Nachhaltiges immobilienmanagement. BBL Berne

Knoeri, C., Sanyé-Mengual, E., and Althaus, H.J. 2013. Comparative LCA of recycled and conventional concrete for structural applications. The International Journal of Life Cycle Assessment, **18**: 909–918. doi:10.1007/s11367-012-0544-2.

Kryžanowski, A., Mikoš, M., Šušteršič, J., Ukrainczyk, V., and Planinc, I. 2012. Testing of concrete abrasion resistance in hydraulic structures on the Lower Sava River. Journal of Materials in Civil Engineering, **58**(4): 245.

Kudale, A.M., Kudale, M.D., and Kulkarni, P.B. 2021. Performance of concrete armour units of breakwaters in India. International Journal of Civil Engineering and Technology, **12**: 54–66. doi:10.34218/IJCIET.12.6.2021.005.

Kumala, Y.E., Lestari, S., and Zulfan, J. 2018. Study to minimize the local scour downstream of Stilling Basin. *In* Proceedings of the 21st Congress of International Association for Hydro-Environment Engineering and Research. Yogyakarta. 2-5 September. pp. 115–122.

Le Franc, M. 1992. Evolution dans l'exploitation des évacuateurs de crues et rénovations récentes sur les barrages d'Electricité de France. La Houille Blanche, **78**(2–3): 163–174. doi:10.1051/lhb/1992014.

Lochon, M., Delhaye, J., Valentini, T., De Cesare, G., and Brühwiler, E. 2024. Hydro-abrasion resistance of UHPFRC and concrete according to the ASTM C1138 method. *In* 10th International Symposium on Hydraulic Structures. Zurich, Switzerland. 17-19 June. pp. 840–849.

Mason, P.J., and Arumugam, K. 1985. Free jet scour below dams and flip buckets. Journal of Hydraulic Engineering, **111**(2): 220–235. doi:10.1061/(ASCE)0733-9429(1985)111:2(220).

Mott, R., Winstral, A., Cluzet, B., Helbig, N., Magnusson, J., Mazzotti, G., et al. 2023. Operational snow-hydrological modeling for Switzerland. Frontiers in Earth Science, **11**. doi:10.3389/feart.2023.1228158.

Parzen, E. 1962. An estimation of a probability density function and model. The Annals of Mathematical Statistics, **33**(3): 1065–1076. doi:10.1214/aoms/1177704472.

Rathod, P., and Manekar, V.L. 2023. Comprehensive approach for scour modeling using artificial intelligence. Marine Georesources & Geotechnology, **41**(3): 312–326. doi:10.1080/1064119X.2022.2035025.

Rosenblatt, M. 1956. Remarks on some nonparametric estimates of a density function. The Annals of Mathematical Statistics, **27**(3): 832–837. doi:10.1214/aoms/1177728190.

Ruiz-Villanueva, V., and Peter, M. 2020. Past, current, and future changes in floods in Switzerland. *In* Hydro-CH2018 project. Commissioned by the Federal Office for the Environment (FOEN), Bern, Switzerland.

Silverman, B.W. 1998. Density estimation for statistics and data analysis. 1st ed. Routledge, New York.

Sixdenier, J.P., Shaiek, S., Erpicum, S., Pirotton, M., and Lahaye, R. 2017. Protection contre l'affouillement du barrage de Poses-Amfreville: études sur modèles réduit et numérique. Hydraulique des barrages et des digues, 142–153.

Wüthrich, D., and Chanson, H. 2014. Hydraulics, air entrainment, and energy dissipation on a Gabion stepped weir. Journal of Hydraulic Engineering, **140**(9): 04014046. doi:10.1061/(ASCE)HY.1943-7900.0000919.

Wuthrich, D., and Chanson, H. 2015. Aeration performances of a gabion stepped weir with and without capping. Environmental Fluid Mechanics, **15**: 711–730. doi:10.1007/s10652-014-9377-9.

Wüthrich, D., Chamoun, S., Bollaert, E., De Cesare, G., and Schleiss, A.J. 2018. Hybrid modelling approach to study scour potential at Chancy-Pougny dam stilling basin. *In* Advances in hydroinformatics: SimHydro 2017. Springer. pp. 869–884. doi:10.1007/978-981-10-7218-5_62.

Wüthrich, D., Chamoun, S., Bollaert, E.F.R., De Cesare, G., and Schleiss, A.J. 2021. Experimental and numerical study on scour-protection methods in a stilling basin: case study of Chancy-Pougny Dam. Journal of Hydraulic Engineering, **147**(6): 05021002. doi:10.1061/(ASCE)HY.1943-7900.0001881.